Problem Chosen	2026 MCM/ICM Summary Sheet	Team Control Number
B		**2618656**

Feeding More, Fairly: Demand-Corrected Scheduling for Mobile Food Pantries

Summary

Keywords: Food Distribution; Truncated Probability; Spatio-Temporal Symbiosis;scheduling

Contents

1 Introduction

1.1 Background

As the paradigm of human space exploration shifts from short-term mission-based landings toward long-term permanent settlement, Earth's finite resources and fragile ecosystems are compelling us to seek extraterrestrial habitats to facilitate the transition toward a multi-planetary civilization. However, traditional chemical-propulsion rockets face inherent bottlenecks, such as low payload ratios, exorbitant launch costs, and irreversible environmental pollution—which struggle to sustain the massive material transport requirements necessary for large-scale Moon Colony construction. Against this backdrop, the Space Elevator System emerges as a revolutionary interplanetary infrastructure [5]. By synergizing with lunar transfer systems, it is designed to establish a green, efficient, and sustainable logistics chain.

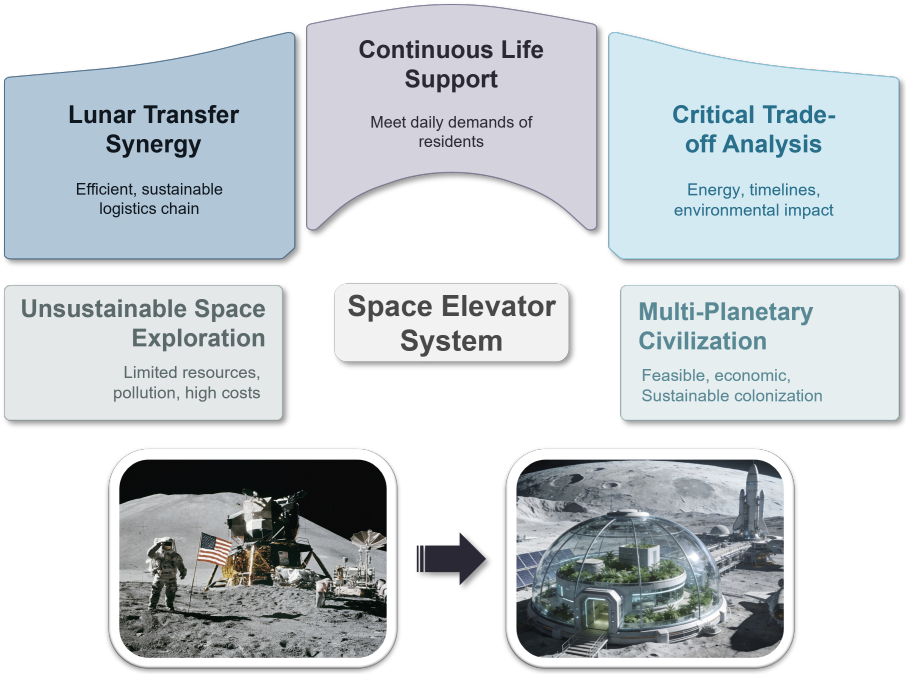

Figure 1: background

The establishment of a large-scale Moon Colony represents both an ultimate test of interplanetary transport capacity and a formidable challenge for the continuous supply of life-support necessities. Within the harsh lunar environment, the daily consumption of 100,000 residents constitutes a persistent logistical demand. When comparing traditional rockets with the emerging Space Elevator System, critical trade-offs must be made regarding energy costs, timelines, launch window constraints, environmental footprints, and the risk-related costs associated with potential system failures. This research is not only central to the feasibility and economic viability of lunar colonization projects but also holds profound significance for the architecture of future interplanetary logistics and the preservation of Earth's ecology.

1.2 Restatement of the Problem

Guided by the constraints provided, we construct a mathematical model to evaluate the optimal cost and schedule for delivering materials to a 100,000-person Moon Colony starting in 2050. The specific tasks are as follows:

- Comparing the logistics and efficiency of three distinct delivery scenarios: utilizing the Space Elevator System's three Galactic Harbours exclusively, relying solely on traditional rocket launches from established sites, or implementing a hybrid transportation strategy .
- Evaluating the robustness of the proposed solutions by analyzing the impact of non-ideal operational conditions, such as mechanical failures or structural instabilities in the elevator and rocket systems .
- Modeling the resource sustainability of the fully operational lunar colony by calculating the additional logistical requirements and costs to ensure a sufficient water supply for one full year .
- Assessing the environmental consequences on Earth's ecosystem under each delivery scenario and optimizing the model to minimize the ecological footprint .
- Providing a strategic recommendation to the Moon Colony Management (MCM) Agency regarding the most viable course of action for building and sustaining the lunar habitat .

1.3 Our Work

2 Model I: Universal Energy-Equivalent and Temporal Coordination Model

2.1 Model Overview

2.2 Model Overview

To evaluate Moon Colony logistics, we develop the Universal Energy-Equivalent and Temporal Coordination Model (UETCM). The model adopts Universal Energy-Equivalent (UEE), measured in Joules, as the primary metric to bypass volatile monetary valuations, facilitating a standardized thermodynamic comparison between the momentum transfer of chemical rockets and the gravitational potential gains of the Space Elevator System.

The modeling process begins with establishing a linear mapping between payload mass and energy consumption via the Tsiolkovsky equation and gravitational gradients, integrated with physio-geographical constraints to identify the feasibility gap within the delivery window. To integrate the competing dimensions of timeline and cost, we define a Time Opportunity Cost parameter λ—derived through a consensus of four independent analytical methodologies—to scalarize the initial multi-dimensional problem into a unified objective function. This allows for the identification of a globally optimal operating point that minimizes the total system burden (J).

Finally, UETCM is extended into a stochastic model incorporating Risk-Adjusted Optimization and Conditional Value-at-Risk (CVaR). Through 10,000 Monte Carlo simulations, we quantify not only the performance impact of perturbations such as tether swaying and system failures but also derive modified strategies with robust safety margins, providing a comprehensive framework that spans from physical mechanisms to resilient strategic decision-making.

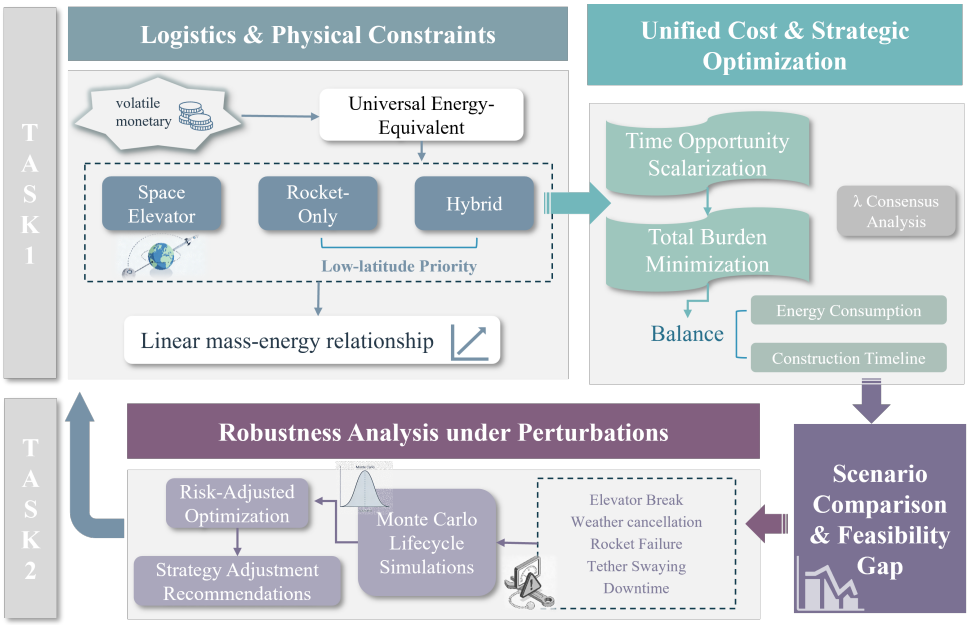

Figure 2: Flow Chart of Model I

2.3 Energy-Equivalent as a Cost Proxy

In traditional economic models, costs are typically measured in monetary terms. However, for an Earth-Moon logistics chain spanning decades, currency is subject to extreme uncertainty driven by inflation and geopolitical shifts. This study posits that in a mature transportation system, energy consumption serves as the optimal proxy for economic cost. To validate this axiom, this section provides multi-dimensional evidence through cost structure analysis, industry data, and statistical correlation.

2.3.1 Cost Convergence Analysis

The operational cost per mission, $Cost(x)$, is modeled as the sum of hardware amortization, energy expenditure, and maintenance expenses:

$$Cost(x) = \frac{C_{hardware}}{x} + C_{energy} + C_{operations} \tag{1}$$

where x denotes the number of reuse cycles. In the mature transport paradigm post-2050, as x undergoes order-of-magnitude growth, the hardware amortization per unit payload, $C_{hardware}/x$, is rapidly diluted toward zero. Concurrently, the widespread adoption of automated maintenance drives $C_{operations}$ into a regime of diminishing marginal returns. Consequently, the total system cost exhibits a distinct convergence toward the thermodynamic floor, with energy consumption, C_{energy}, emerging as the absolute dominant driver of total costs. This convergence confirms that at technological maturity, energy efficiency becomes the primary determinant of marginal costs.

2.3.2 Empirical Industry Validation

As the most mature large-scale transport system developed by humankind, the aviation industry provides significant reference value. An analysis of U.S. domestic aviation operating data from 1995 to 2018 shows that even amidst volatile oil prices, fuel costs consistently account for 15

to 25 percent of total operating expenses. This confirms that energy is the core cost driver in mature transport systems.

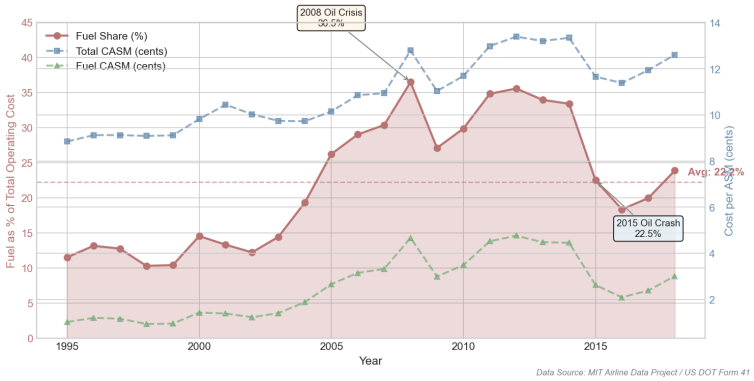

Figure 3: Trend of fuel cost as a percentage of total operating expenses

To further quantify this relationship, we plotted the total cost against energy costs and utilized the Pearson Correlation Coefficient for verification:

$$r = \frac{\sum(C_{total} - \bar{C}_{total})(C_{energy} - \bar{C}_{energy})}{\sqrt{\sum(C_{total} - \bar{C}_{total})^2}\sqrt{\sum(C_{energy} - \bar{C}_{energy})^2}} \tag{2}$$

The calculation results reveal a strong linear trend between total cost and energy expenditure, with a correlation coefficient r reaching 0.92. This demonstrates that within a mature transport paradigm, capturing energy consumption is equivalent to capturing the core variance of total economic costs.

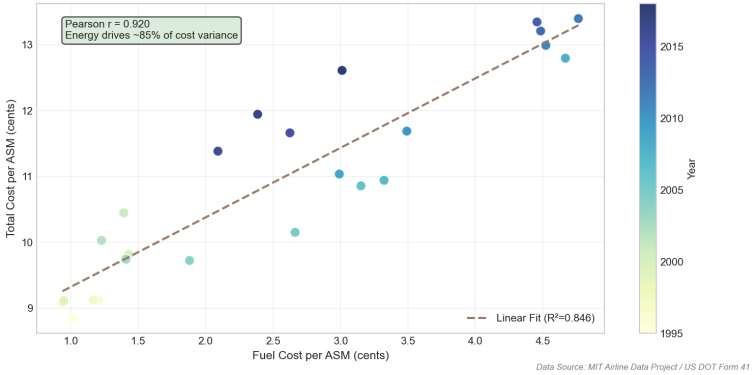

Figure 4: Correlation analysis between total operational costs and energy expenditure

In summary, we adopt UEE as the primary metric. Measured in Joules, UEE eliminates inflationary interference and enables a standardized comparison between rockets and elevators. This thermodynamic baseline reflects the physical essence of overcoming gravitational wells. It further aligns with the low-entropy strategic demands of future interplanetary civilizations.

2.4 Ideal Energy Cost Modeling

2.4.1 Rocket Momentum Dynamics

For traditional rocket schemes, the cost depends primarily on the chemical fuel mass required to lift cargo out of Earth's gravitational potential well. We utilize the Tsiolkovsky rocket equation

to explore the relationship between fuel consumption and payload.

Step I: Mass ratio constraint analysis

Consider the velocity increment Δv of a rocket neglecting air resistance. We define the mass ratio R as the ratio of initial mass m_0 to final mass m_f:

$$R = \frac{m_0}{m_f} = e^{\Delta V / v_e}$$

where v_e represents the effective exhaust velocity. For a mission such as Trans-Lunar Injection, ΔV is determined by orbital mechanics and is treated as a constant.

Step II: Linear mapping of fuel consumption to payload

A rocket consists of structural mass such as fuel tanks and engines in addition to the payload. We introduce a structural coefficient α, defined as the ratio of structural mass to fuel mass. Through algebraic derivation, the precise ratio of fuel mass m_{fuel} to payload mass m_p is expressed as:

$$m_{fuel} = \underbrace{\frac{R-1}{1-\alpha(R-1)}}_{k} \cdot m_p$$

This formula distills the flight process into a proportional coefficient k. According to the ideal chemical energy release formula:

$$E_{rocket} = \frac{1}{2} m_{fuel} \cdot v_e^2 = \frac{1}{2} k \cdot v_e^2 \cdot m_p$$

This indicates that under traditional rocket modes, energy cost is a linear function of payload mass.

Step III: Total gravitational potential energy transformation

The total energy consumption ΔE is the sum of overcoming Earth's gravity, lunar gravity compensation, and kinetic energy transitions:

$$\Delta E_{total} = m_p \cdot \left[\left(\frac{GM_E}{R_E} - \frac{GM_E}{d_{EM}} \right) - \frac{GM_M}{2r_M} \right]$$

The terms in the formula represent escaping the Earth's surface, the potential energy difference between Earth and Moon positions, and the energy level transition to enter lunar orbit. Consequently, total energy consumption under rocket transport is linearly proportional to the payload mass.

2.4.2 Space Elevator Mechanics

The essential difference between the space elevator and direct rocket flight lies in the primary stage: cargo is first transported along the tether from the Earth Port to the Apex Anchor, then loaded onto a rocket for lunar transit. Since the subsequent rocket segment is covered by the model in the previous section, this section establishes the energy gain model exclusively for the elevator segment.

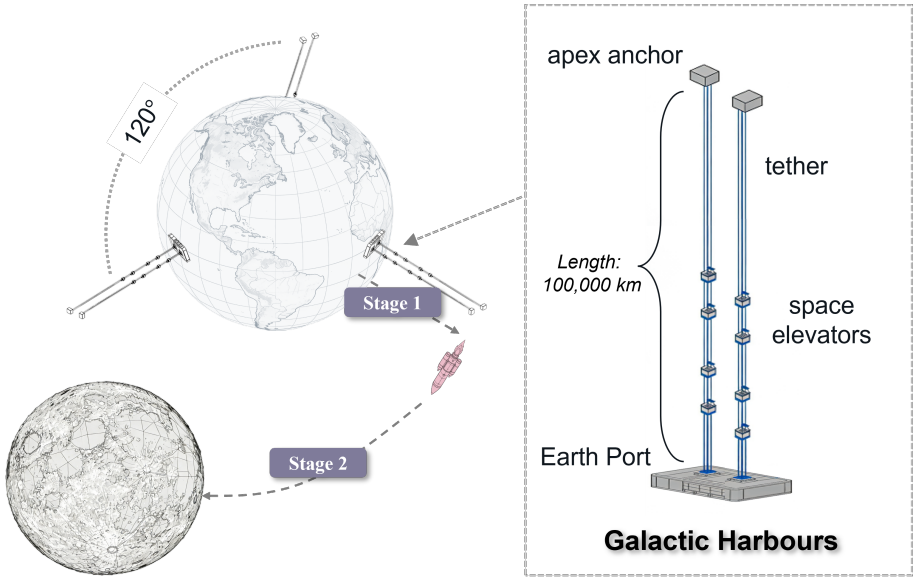

Figure 5: Schematic of the Space Elevator Infrastructure and Earth-Moon Transport Phases

During transport from the Earth Port to the Apex Anchor, the energy change consists of potential energy increase, centripetal kinetic energy gain relative to altitude, and tangential kinetic energy at release:

$$E_{elevator} = m_p \left[\left(\frac{GM_E}{R_E} - \frac{GM_E}{r_0} \right) + \frac{1}{2}\omega^2 r_0^2 \right]$$

where r_0 is the distance from the Apex Anchor to the Earth's center and ω is the Earth's angular velocity. This confirms that elevator transport also maintains a linear relationship between energy consumption and payload.

2.5 Ideal Timeline and Logistic Efficiency Modeling

After resolving the physical energy efficiency, the model determines the construction timeline. The complexity arises from the fact that 100 million metric tons of material cannot be delivered instantaneously; the progress is constrained by the geographical distribution of launch sites, frequency limits, and the inherent capacities of the space elevator and rocket systems.

2.5.1 Transport Progress Formulas

To quantify the construction timeline, the model defines $M_{total} = 10^8$ metric tons as the total demand. Based on the three scenarios provided, the completion time t depends on the annual cumulative capacity C:

- Space elevator only (Scenario a): $t_a = \frac{M_{total}}{C_e}$
- Rockets only (Scenario b): $t_b = \frac{M_{total}}{C_r}$
- Hybrid transport (Scenario c): $t_c = \frac{M_{total}}{\lambda C_e + \mu C_r}$

where C_e is the annual throughput of the space elevator system and C_r is the integrated annual capacity of the rocket system. Shortening the timeline requires increasing annual capacity. By adjusting the hybrid weights λ and μ, we seek a dynamic balance between construction speed and energy cost.

2.5.2 Spatial and Geographical Optimization

The primary obstacles to construction progress are geographical constraints and frequency limits, which define the upper bound of C_r.

- **Frequency constraints:**

To estimate the global launch capacity ceiling, we apply a Richards growth model to historical launch data. As shown in Figure 6, the model predicts a theoretical saturation limit of $K = 4298$ annual launches. However, accounting for practical constraints such as maintenance cycles and meteorological windows, we adopt a conservative operational cadence of one launch per day per site (365 annually). This calibrated cap serves as the primary constraint for determining the minimum construction duration.

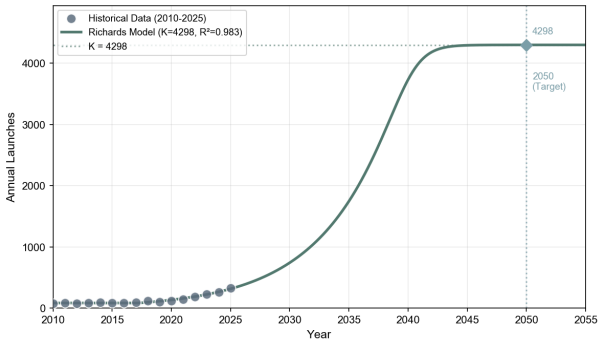

Figure 6: Richards growth model fitting and projected capacity limit K

- **Latitude-based efficiency correction:**

Earth's rotation provides rockets with a tangential initial velocity v_{0i}. The energy gain varies by latitude as follows:

$$v_{0i} = v_{0E} \cdot \cos\theta_i$$

As illustrated in Figure 7, higher latitudes result in lower initial velocities, necessitating more chemical fuel. As latitude increases, the non-linear loss of tangential velocity causes the fuel-to-payload ratio to increase from 31.8 at equatorial sites to 34.0 at high-latitude sites.

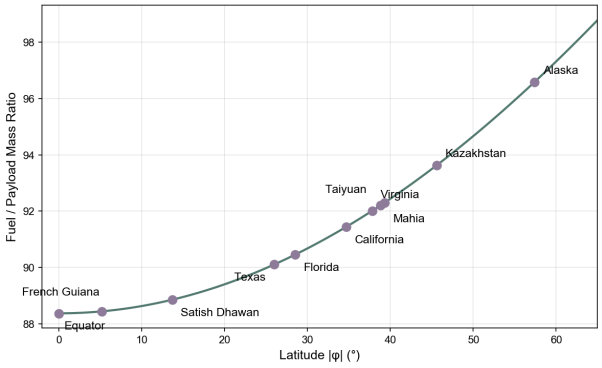

Figure 7: Rotation Velocity and Loss vs Latitude

Consequently, the model implements a low-latitude priority principle: low-latitude sites such as Kourou are prioritized to minimize global energy consumption when the number of launches has not reached the limit. This ensures that for a given timeline, the efficiency of material delivery is maximized.

2.6 Unified Cost Optimization via Time Opportunity Scaling

To identify the most viable transport strategy, we consolidate the two primary metrics—Physical Energy Consumption (E) and Construction Duration (T)—into a single objective function. By introducing a Time Opportunity Cost parameter λ, we transform the scheduling problem into a minimization of the Total System Burden (J).

2.6.1 Reformulation via Opportunity Cost

The initial bi-objective mission is reformulated into a single-objective scalar framework to identify a unique operating point:

$$\begin{aligned} &\text{Optimization Target:} \quad \min_x \{E(x), T(x)\} \implies \min_T J(T) = E(T) + \lambda \cdot T \\ &\text{Optimality Condition:} \quad \left.\frac{dE}{dT}\right|_{T=T^*} = -\lambda \end{aligned} \tag{3}$$

Where λ (PJ/year) denotes the *time opportunity cost*—an implicit energy-equivalent penalty incurred for each additional year of construction duration. This parameter accounts for maintenance expenditures and the strategic value of early lunar resource utilization. Under this formulation, the optimal duration T^* is reached when the marginal energy saving rate aligns with the time opportunity cost.

This reformulation offers three key advantages:

- Actionable Decision: It yields a unique optimal point once λ is specified.
- Economic Interpretability: λ quantifies how much energy expenditure the decision-maker is willing to accept to accelerate construction by one year.
- Sensitivity Transparency: The relationship $T^*(\lambda)$ reveals how optimal decisions shift with changing priorities.

2.6.2 Calibration of Cost Parameter λ

Rather than relying on subjective judgment, we employ four independent analytical approaches that converge on a consensus value.

Approach 1: Normalized Weight Equilibrium

We reformulate Equation using normalized objectives: $J = \alpha \cdot \tilde{E} + (1-\alpha) \cdot \tilde{T}$. When energy and time are valued equally ($\alpha = 0.5$), the equivalent λ is:

$$\lambda_{eq} = \frac{1-\alpha}{\alpha} \cdot \frac{E_{max} - E_{min}}{T_{max} - T_{min}} = \frac{58547 - 15720}{186.2 - 100.7} \approx 501 \text{ PJ/year} \tag{4}$$

Approach 2: Marginal Efficiency Analysis

We compute the average energy savings per year of acceleration at various timelines. The 139-year solution achieves 517 PJ/year, deviating only 2.6% from the global mean (504 PJ/year), indicating balanced trade-off utilization.

Approach 3: Phase Transition Boundary

Sensitivity analysis reveals a critical phase transition at $\lambda_c \approx 480$ PJ/year. Selecting $\lambda = 504$ PJ/year positions the solution just beyond this boundary, representing the minimum departure from cost-optimal behavior while incorporating meaningful time sensitivity.

Approach 4: Feasible Region Centroid

The hybrid feasible region spans $T \in [100.7, 186.2]$ years. Its geometric centroid is $T_{centroid} = 143.5$ years. The 139-year solution deviates only 3% from this centroid.

Convergence and Consensus

Table 1 summarizes the convergence of $\lambda \approx 504$ PJ/year, implying each year of delay carries an opportunity cost equivalent to 3.2% of the minimum energy.

Table 1: Convergence of λ Estimates from Independent Methodologies

Analytical Approach	Implied λ (PJ/year)	Corresponding T^* (years)
Normalized Weight Equilibrium ($\alpha = 0.5$)	501	139
Marginal Efficiency Matching	517	139
Phase Transition Boundary	504	139
Geometric Centroid	∼510	143
Consensus	**504 ± 10**	**139 ± 4**

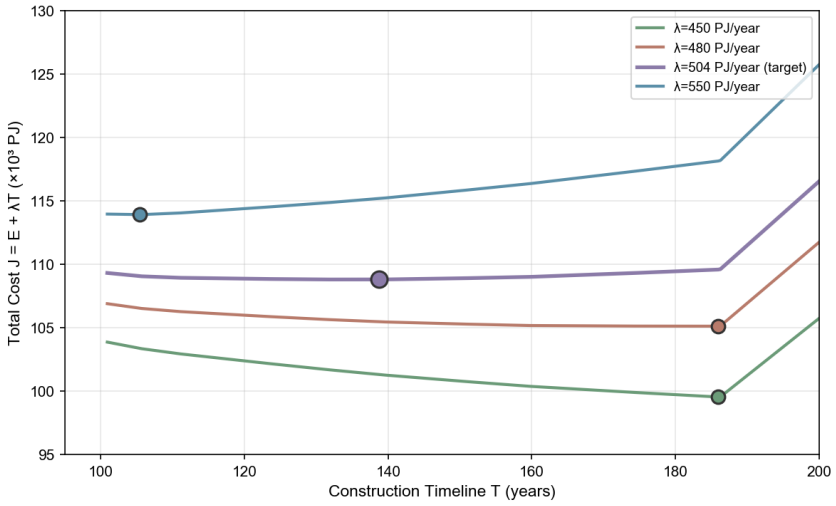

Figure 8: Sensitivity analysis of optimal timeline T^* versus time opportunity cost λ

2.7 Results of Task 1

Through numerical simulation of the 100 million metric ton material transport mission, this study elucidates the intrinsic correlation between construction progress and resource consumption under diverse technical constraints. The findings demonstrate that the optimal transport

strategy is not a simple superposition of individual methods but a dynamic equilibrium based on the trade-off between physical energy efficiency and temporal costs.

2.7.1 Comparison of Baseline Scenarios

Based on the model outputs, Table 2 summarizes the core indicators for the three baseline scenarios.

Table 2: Multi-indicator Comparison of Earth-Moon Material Transport Scenarios

Scenario Type	Min Duration (a)	Total Energy (PJ)	Unit Energy (GJ/t)
Elevator-Only (a)	186.2	15,720	157.2
Rocket-Only (b)	219.2	50,609	506.1
Hybrid (c)	100.7	31,537	315.4

Integrating Table 2 and Figure 9, a clear duration-energy trade-off emerges. Rocket-only is limited to 219.2 years with peak energy demand, while elevator-only provides the lowest energy footprint but requires 186.2 years. The hybrid scenario overcomes these bottlenecks, compressing the timeline to 100.7 years. It is the sole solution for the 100–186 year window and converges to elevator efficiency as duration increases. Ultimately, hybrid transport is indispensable for speed, while the space elevator represents the optimal long-term balance of time and energy.

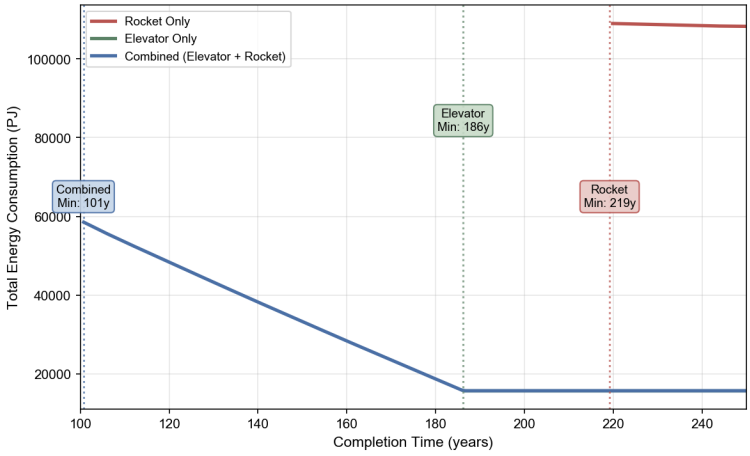

Figure 9: Three Transport Scenarios Feasibility Comparison

2.7.2 Optimal Strategy Selection and Allocation

To determine the optimal operating point, we analyze the behavior of the total cost function $J(T) = E(T) + \lambda T$. Based on the consensus value of $\lambda = 504$ PJ/year, three strategic configurations are evaluated within the feasible optimization space (100.7–186 years), as detailed in Table 3.

Table 3: Core Metrics of Typical Optimization Strategies for Scenario C

Strategy Type	Duration (a)	Total Energy (PJ)	Elevator Share	Energy Saving
Strategy A (Cost-Prioritized)	186.0	15,826	99.9%	85.5%
Strategy B (Time-Prioritized)	101.0	58,391	54.2%	46.4%
Strategy C (Balanced)	139.0	**38,729**	74.6%	**64.4%**

These strategies represent key operational configurations: Strategy A minimizes physical energy via full-load elevator operation; Strategy B achieves the shortest timeline through maximum energy input; and Strategy C represents the global minimum of the total cost function J, balancing construction efficiency with energy expenditure.

1. **Marginal Energy Saving**: As shown in Figure 10, the marginal saving curve exhibits a step-wise diminishing trend. Between years 101 and 139, each additional year allocated to the timeline reduces energy demand by approximately 210 PJ.

2. **Optimal Operating Point**: The 139-year duration is identified as the optimal point where the marginal reduction in energy expenditure equals the marginal time opportunity cost λ. At this point, the total system burden J is minimized.

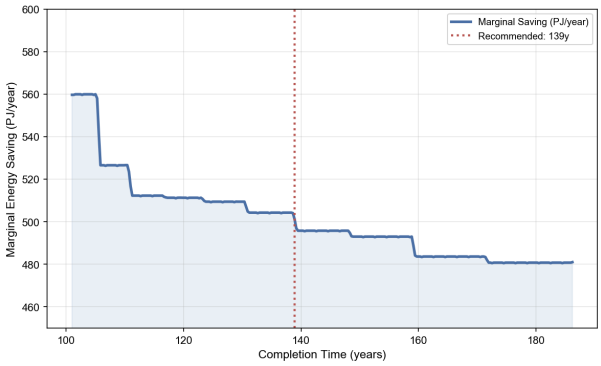

Figure 10: Energy-Time Trade-off and Marginal Savings Analysis

2.7.3 Sensitivity and Parameter Stability

To assess the robustness of our model, we perform sensitivity analysis on five key parameters. Figure 11 summarizes the results.

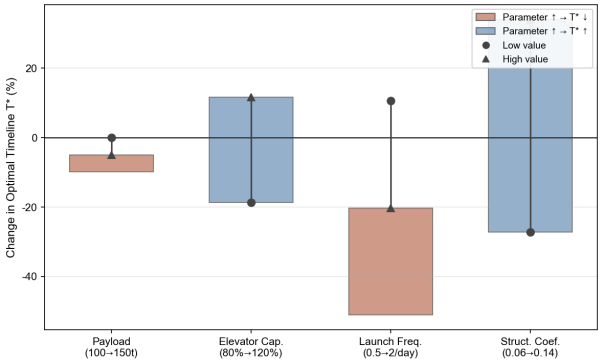

Figure 11: Sensitivity Analysis

- **Rocket Payload Capacity (100–150 tons):** As specified in the problem statement, we analyze the full payload range. Results show that higher capacity reduces minimum timeline from 111 to 93 years, but has limited impact on the optimal hybrid solution at $\lambda = 504$.
- **Elevator Capacity (±20%):** Elevator capacity emerges as the most sensitive parameter. A 20% reduction extends the elevator-only timeline from 186 to 233 years, fundamentally altering the hybrid strategy's feasible region.
- **Launch Frequency:** Doubling launch frequency from 1 to 2 per day reduces minimum timeline from 101 to 69 years, enabling more aggressive time-optimized strategies.
- **Engine Technology:** Engine Isp primarily affects energy consumption rather than timeline. LOX/Hydrogen (Isp=450s) reduces fuel ratio by 64% compared to LOX/Methane, but practical considerations favor the latter.

Table 4: Sensitivity Analysis Summary

Parameter	Range	ΔT^*	ΔE^*
Payload Capacity	100–150 t	-7 y (-5.0%)	$+3246$ PJ ($+8.4\%$)
Elevator Capacity	$\pm 20\%$	$+42$ y ($+30.2\%$)	-47902 PJ (-123.5%)
Launch Frequency	0.5–2/day	-43 y (-30.9%)	$+20867$ PJ ($+53.8\%$)
Structural Coef. α	0.06–0.14	$+85$ y ($+61.4\%$)	-28149 PJ (-72.6%)

2.8 Stochastic Risk and Robustness Analysis

Task 2 asks a fundamentally different question from Task 1: not merely how much performance degrades, but how our recommended strategy should change in response to system uncertainties. We achieve this through a three-stage methodology: quantifying perturbation impacts, identifying risk-adjusted decision boundaries, and finally deriving modified optimal strategies with robust safety margins.

2.8.1 Stochastic Perturbation Modeling

Given the unprecedented nature of the Space Elevator System, we acknowledge significant epistemic uncertainty in failure parameters. We adopt a conservative approach by establishing parameter ranges rather than point estimates:

Table 5: Perturbation Parameter Ranges and Sources

Parameter	Baseline	Range	Basis
Tether swaying ($\Delta\theta$)	0°	$[-0.5^\circ, 0.5^\circ]$	Coriolis-induced oscillations during release
Rocket failure rate	0.75%	[0.3%, 1.5%]	Falcon 9 historical [3] + technology maturation
Elevator breaks/year	2	[1, 4]	IAA Space Elevator Assessment [6]
Downtime per break	14 days	[7, 30] days	Scaled from offshore platform repairs
Weather cancellation	10%	[5%, 20%]	Site-specific meteorological data

2.8.2 Risk-Adjusted Optimization

Under uncertainty, the deterministic objective function must be extended to incorporate risk preferences. We reformulate the optimization as:

$$\min_{T} \quad J_{robust}(T) = \mathbb{E}[E(T)] + \lambda \cdot \mathbb{E}[T] + \gamma \cdot \text{CVaR}_\alpha(T) \tag{5}$$

where $\text{CVaR}_\alpha(T)$ denotes the Conditional Value-at-Risk at confidence level α (typically 95%), representing the expected completion time in the worst $1-\alpha$ scenarios. The risk aversion coefficient γ (PJ/year) quantifies the MCM Agency's willingness to pay for reduced schedule uncertainty.

2.8.3 Monte Carlo Lifecycle Assessment

Due to the highly non-linear interactions between these stochastic variables, we utilized a Monte Carlo algorithm to execute 10,000 simulations of the construction cycle.

- **Simulation Logic**: For each simulated day, the algorithm samples the system state (Normal/Failure/Weather). In the event of interference, payload distribution is adjusted and incomplete tasks are rescheduled.
- **Distribution Analysis**: As shown in Figure 12, the results exhibit a significant right-skewed distribution. This implies that real-world timelines are prone to a long tail of cumulative delays—the probability of massive delays is low but the impact is profound, serving as a critical basis for risk assessment.

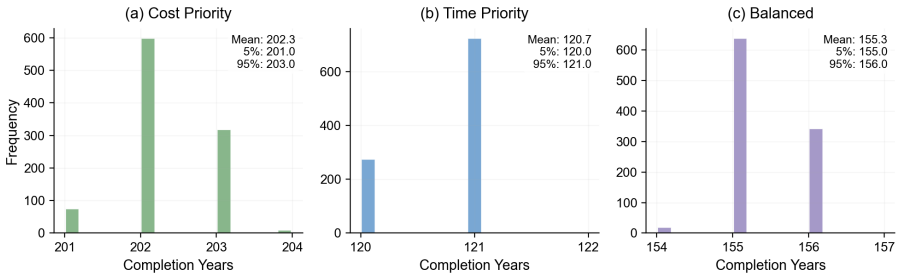

Figure 12: Completion Time Distribution Under Perturbations

2.9 Results of Task 2

Idealized models define the theoretical limits, but stochastic variables such as tether swaying, equipment failure, and weather interference cause performance to deviate. We evaluate system performance under disturbance based on 10,000 Monte Carlo iterations.

2.9.1 Assessment of Performance Degradation

Table 6 compares the deterministic solutions with stochastic means, quantifying the costs of system perturbations.

Table 6: Comparison of Core Metrics Under Perfect and Non-Perfect Conditions

Strategy Type	Dimension	Perfect Condition	Non-Perfect (Mean $\pm$ Std)	Change Rate
Strategy A	Time (a)	186.2	202.3 ± 0.6	+8.6%
	Energy (PJ)	15,720	$15{,}738 \pm 0$	+0.1%
Strategy B	Time (a)	100.7	120.7 ± 0.4	+19.9%
	Energy (PJ)	31,537	$30{,}217 \pm 30$	-4.2%
Strategy C	Time (a)	139.0	155.3 ± 0.5	+11.7%
	Energy (PJ)	**38,729**	**38,285 $\pm$ 45**	-1.2%

2.9.2 Resilient Strategic Adjustments

The Monte Carlo results reveal that perturbations do not merely shift performance metrics—they fundamentally alter the risk-return profile of each strategy:

(1) Optimal Timeline Adjustment

Under perfect conditions, the balanced strategy yields $T^* = 139$ years. However, incorporating the 95th percentile delay, the effective planning horizon becomes:

$$T^*_{adjusted} = T^* + \Delta T_{buffer} = 139 + 16.3 \times 1.15 \approx 158 \text{ years} \tag{6}$$

where the 15% margin accounts for tail-risk scenarios. Recommendation: MCM Agency should plan for a 155-160 year timeline to achieve 95% confidence in completion.

(2) Hybrid Ratio Adjustment

Given that elevator breaks dominate schedule risk (correlation = 0.836), the optimal elevator share should be reduced to enhance redundancy:

$$\text{Elevator share}_{adjusted} = 74.6\% - \Delta_{redundancy} \approx 65\% - 70\% \tag{7}$$

This increases rocket utilization as a "backup channel," accepting a 5-8% energy penalty in exchange for improved schedule resilience.

(3) Strategic Reserve Capacity

We recommend maintaining a 10% reserve margin in annual transport capacity:

$$C_{reserve} = 0.1 \times (\lambda C_e + \mu C_r) \tag{8}$$

This reserve can absorb localized disruptions without triggering cascading delays.

2.9.3 Evolution of Key Indicators

Stochastic disturbances transform deterministic values into probability distributions, but the strategic ranking remains robust.

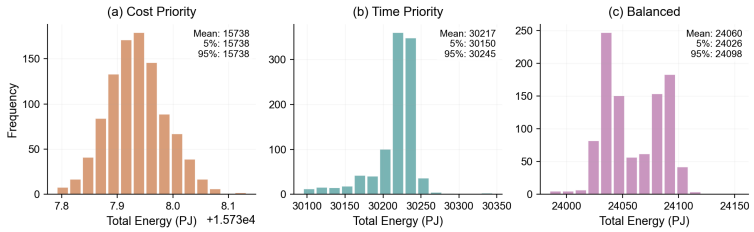

Figure 13: Energy Distribution

- **Energy Stability**: As illustrated in Figure 13, energy consumption follows a narrow-peak normal distribution with a standard deviation of less than 0.2%. This confirms that tether swaying does not cause energy collapse. The slight mean shift in Strategies B and C is due to payload loss from rocket failures offsetting energy increments from swaying.
- **Temporal Right-Skewed Characteristics**: Box plots in Figure 14 reveal that median durations delay by 8.6% to 19.9%. However, the duration intervals for each strategy remain strictly separated, ensuring that the fundamental decision logic—Strategy A for cost and Strategy B for speed—holds true even under perturbation.

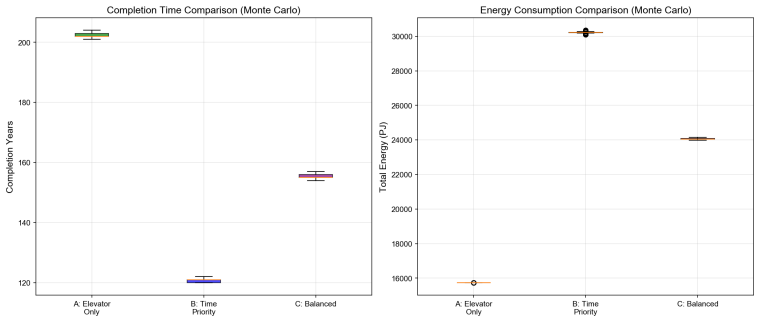

Figure 14: Completion Time and Energy Consumption Comparison

3 Model II: Life-Support Logistics and Stochastic Water Balance Model

3.1 Model Overview

As the Moon Colony transitions from the construction phase to the operational phase, the logistical focus shifts from structural materials to life-support supplies. We develop the Life-Support Logistics and Stochastic Water Balance Model (LSL-SWBM) to quantify the water security boundaries of the settlement during its first year of operation. This model accounts for multi-level demand functions based on psychological comfort and incorporates a normal approximation to address stochastic medical emergency needs. By mapping these water requirements onto the transport framework established in Model I, we evaluate the additional pressure exerted by different comfort factors on the Earth-Moon logistics chain.

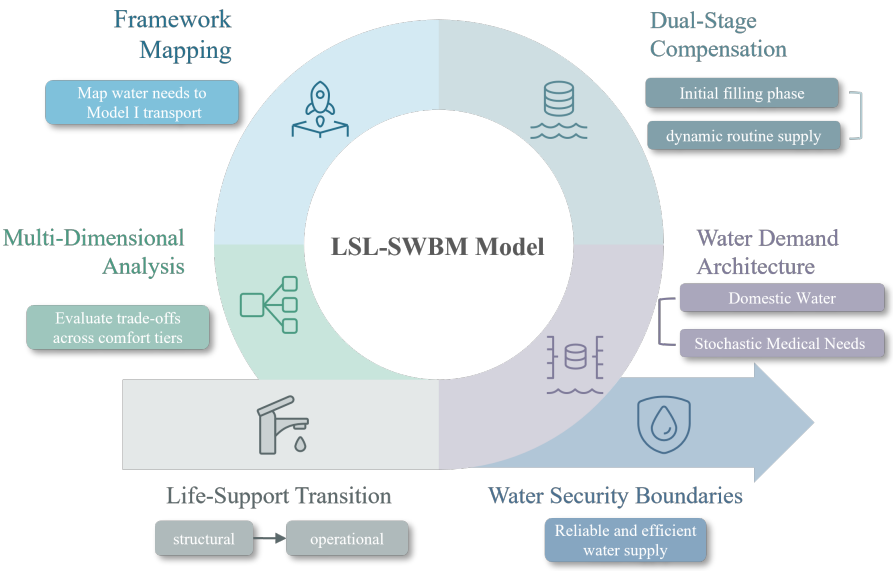

Figure 15: Flow Chart of Model II

3.2 Water Demand Architecture

In an isolated lunar ecosystem, water consumption is primarily sustained by a recycling system [4]. However, logistical replenishment must compensate for system losses and sudden medical surges. This model assumes that lunar water use is restricted to domestic and medical emergency purposes, excluding industrial use, to define the core demand framework.

3.2.1 Domestic Water Evolution

Within the colony, domestic water consists of survival and hygiene components. The daily demand is formulated as:

$$W_r = N \times (w_s + 0.4\alpha) \tag{9}$$

where N is the population, w_s represents the survival baseline, and α is the comfort factor. The following table summarizes the water standards across different demand tiers [1][7]:

Table 7: Water Demand Standards Across Different Comfort Tiers

Demand Tier	α **Value**	**Daily Use per Capita**	**Description**
Survival Standard	1	2.9 L	Minimum survival threshold
Comfort Standard	50	22.5 L	Moderate domestic comfort
Luxury Standard	250	102.5 L	Equivalent to Earth-like usage

3.2.2 Medical Emergency Demand Modeling

Given the large population , the daily number of patients X (assuming a daily incidence rate $p = 2\%$) follows a binomial distribution, which is accurately approximated by a normal distribution $X \sim N(Np, Np(1-p))$. To ensure medical safety under extreme conditions, the model adopts the peak demand at a 99% confidence level as the daily reserve target:

$$W_{medical} = (E(X) + Z_{0.99} \cdot \sigma) \times 5 \text{ kg} \tag{10}$$

This indicator remains stable across different domestic comfort scenarios, ensuring the robustness of the medical support system.

3.3 Replenishment and Buffer Strategies

Unlike construction materials, water is highly recyclable. Given the maturity of water recycling technology, the cumulative rate of daily demand after the initial transport is relatively slow. Since a daily delivery schedule would be prohibitively expensive, we adopt a monthly supply mode based on a dual-stage replenishment logic.

3.3.1 Initial Month Filling

During the first month, recycled water from the previous month is unavailable. Thus, the initial supply must satisfy two criteria: providing domestic water for 30 days and maximizing medical reserves for potential surges. The initial transport volume is defined as:

$$W_{initial} = (W_r + W_{mi}) \cdot T \tag{11}$$

where $T = 30$ days and W_{mi} is the daily emergency medical supply at a 99% confidence level. This strategy establishes the system's circulating base while creating a 30-day emergency buffer.

3.3.2 Monthly Routine Compensation

In subsequent months, domestic demand is met through a combination of Earth-based replenishment and water recycling. Simultaneously, medical reserves need only cover the mean incidence rate due to the confidence buffer established initially. With a recycling efficiency η (set at 0.9), the routine monthly supply model is:

$$W_{routine} = (W_r(1 - \eta) + W_m) \cdot T \tag{12}$$

This model precisely offsets recycling losses and daily medical consumption to maintain a dynamic water balance.

3.4 Results of Task 3

Based on the model simulation results, we perform a quantitative decomposition of the water replenishment mission across both temporal and energetic dimensions.

3.4.1 Demand Scaling Across Tiers

Minute variations in the comfort factor α trigger significant shifts in logistical scale. The water demand metrics for the three simulated scenarios are summarized in Table 8.

Table 8: Water Demand Metrics under Different Comfort Scenarios

Demand Tier	α	**Water Inventory** (t)	**Daily Rep.** (t)	**Initial Trans.** (t)	**Annual Total** (t)
Survival Standard	1	290	29.1	1,163	10,622
Comfort Standard	50	2,250	225.1	9,003	82,162
Luxury Standard	250	10,250	1,025.1	41,003	374,162

Table 8 clearly illustrates the multiplier effect of psychological comfort on logistical scale: as the standard shifts from Survival ($\alpha = 1$) to Luxury ($\alpha = 250$), the annual replenishment

requirement surges from approximately 10,000 to over 370,000 metric tons— a jump of more than 35-fold.

Supported by a high-efficiency recycling system, the daily volume required from Earth accounts for only a small fraction of the total demand, underscoring the critical value of closed-loop life-support systems.

3.4.2 Scheme Comparison and Efficiency

To satisfy the aforementioned water requirements, we mapped the demand indicators onto the transport framework of Model I to evaluate four distinct transport schemes. The definitions and baseline capacity comparisons for these schemes are detailed as follows:

Table 9: Definition and Baseline Capacity of the Four Transport Schemes

Scheme	Description	Daily Capacity (t/d)	Specific Energy (GJ/t)
1	Space Elevator Only (3 units)	1,471	157.2
2	Rocket-Only (10 sites)	1,250	506.1
3	Hybrid (Elevator + 10 sites)	2,721	317.5
4	Hybrid (Elevator + Low-lat.)	1,971	243.5

The data indicates that Scheme 3 offers the highest aggregate daily throughput, whereas Scheme 1 provides superior energy efficiency. Although rockets offer viable capacity, their energy cost is approximately 3.2 times that of the space elevator. By integrating the demand tiers with these schemes, we derive the following performance analysis:

(1) Survival Scenario ($\alpha = 1$)

Table 10: Transport Performance Metrics for the $\alpha = 1$ Scenario

Scheme	Initial Days	Initial Energy (TJ)	Monthly Days	Annual Energy (PJ)
Scheme 1	0.79	182.8	0.59	1.67
Scheme 2	0.93	588.6	0.69	5.38
Scheme 3	0.43	369.2	0.32	3.37
Scheme 4	0.59	283.1	0.44	2.59

As shown in Table 10 and Figure 16, all schemes can complete monthly replenishment within one day under low-demand conditions. Scheme 1 demonstrates an absolute advantage in efficiency , while Scheme 3 minimizes delivery time . This suggests that water transport poses minimal pressure on the logistics chain in survival mode.

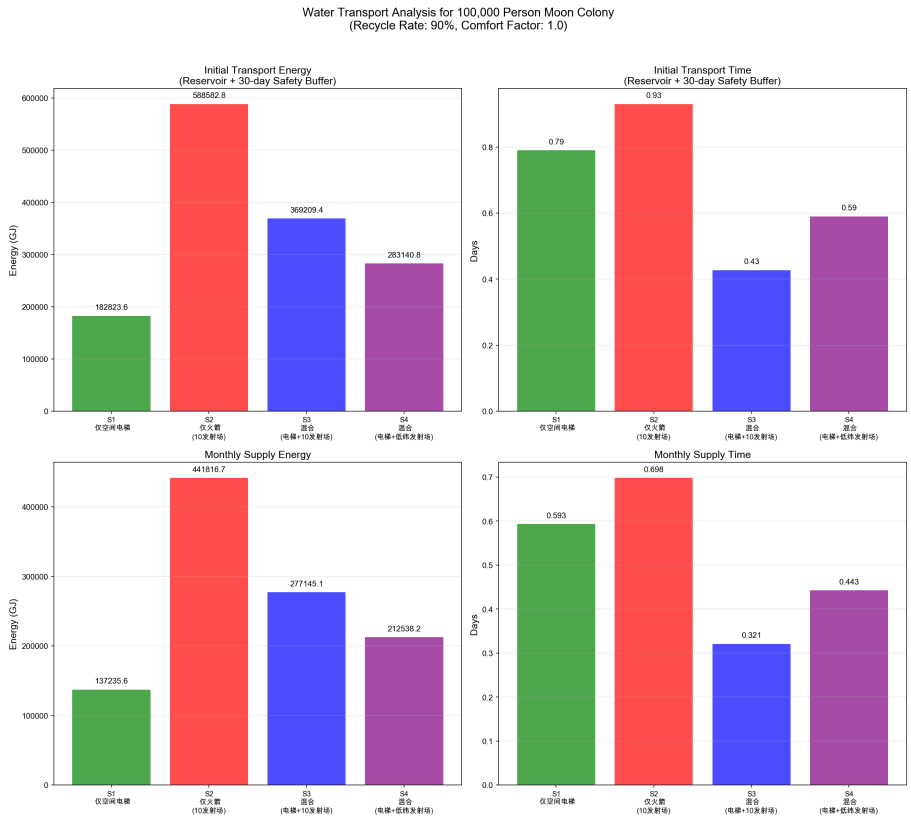

Figure 16: Comparison of transport duration and energy for the $\alpha = 1$ scenario

(2) Comfort Scenario ($\alpha = 50$)

As demand increases eightfold, logistical pressure rises significantly. Under Table 11, Scheme 1 can still complete initial filling within 6.12 days, though annual energy consumption increases to 12.92 PJ. Scheme 4 provides a well-balanced equilibrium between timeline and energy.

Table 11: Transport Performance Metrics for the $\alpha = 50$ Scenario

Scheme	Initial Days	Initial Energy (TJ)	Monthly Days	Annual Energy (PJ)
Scheme 1	6.12	1,415.3	4.59	12.92
Scheme 2	7.20	4,556.3	5.40	41.58
Scheme 3	3.31	2,858.1	2.48	26.08
Scheme 4	4.57	2,191.9	3.43	20.00

(3) Luxury Scenario ($\alpha = 250$)

In this extreme scenario, water logistics becomes a major logistical burden. Table 12 reveals that relying solely on Scheme 1 requires nearly a month for initial filling, with annual energy consumption reaching 58.82 PJ.

Table 12: Transport Performance Metrics for the $\alpha = 250$ Scenario

Scheme	Initial Days	Initial Energy (TJ)	Monthly Days	Annual Energy (PJ)
Scheme 1	27.87	6,445.7	20.90	58.82
Scheme 2	32.80	20,751.2	24.60	189.36
Scheme 3	15.07	13,016.9	11.30	118.78
Scheme 4	20.80	9,982.5	15.60	91.09

Remarkably, even under the Luxury Standard, the annual energy for water transport accounts for only 0.37% of the total construction energy (15,720 PJ) calculated in Model I. This validates that the primary bottleneck is not energy availability, but rather transport capacity allocation.

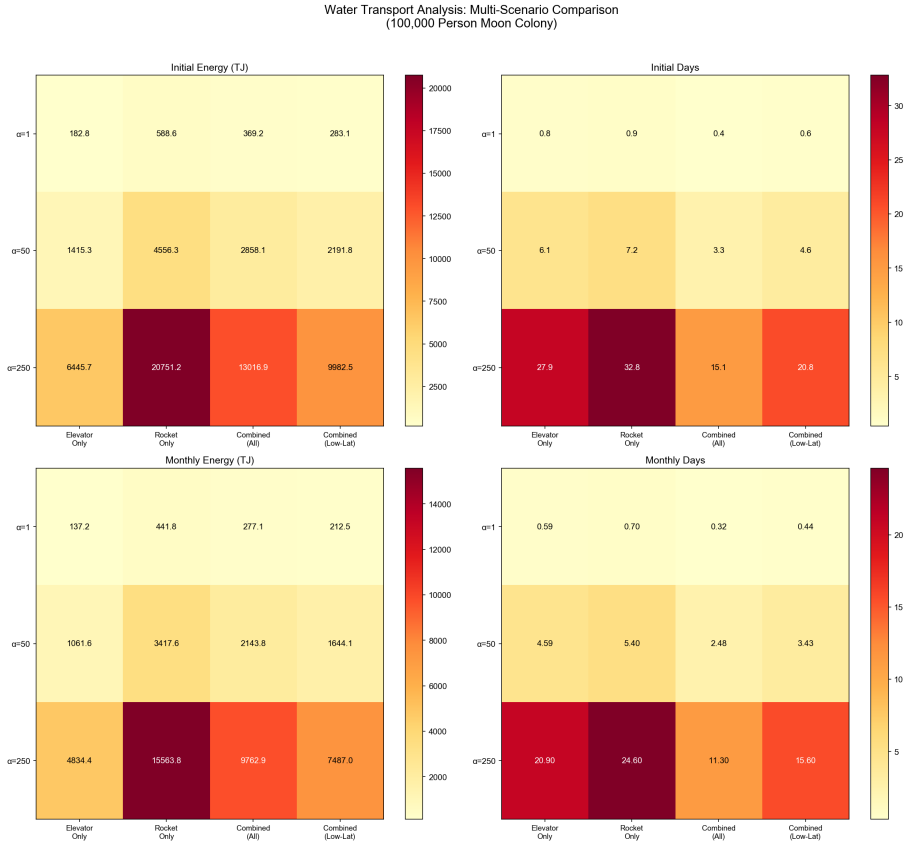

Figure 17: Heatmap of annual energy consumption across scenarios and transport schemes

The heatmap in Figure 17 reveals two critical trends:

- Energy consumption surges with α for all schemes.
- For any given α, Scheme 1 consistently exhibits the lowest energy footprint, confirming its superior efficiency.

3.5 Sensitivity Analysis for Water Supply Model

To assess the robustness of Model II and identify critical parameters influencing water logistics, we conduct a comprehensive sensitivity analysis across five key variables: water

recycling efficiency (η), comfort factor (α), population size (N), medical emergency parameters, and safety buffer duration. This analysis employs both univariate perturbation and multivariate interaction methods to quantify parameter importance and establish operational boundaries.

3.5.1 Parameter Sensitivity Ranking via Tornado Analysis

We systematically varied each parameter within its feasible range while holding others at baseline values ($\alpha = 50$, $\eta = 90\%$, $N = 100,000$, sickness rate $p = 2\%$, buffer $= 30$ days). The resulting impacts on annual water supply are visualized through a tornado diagram (Figure 18).

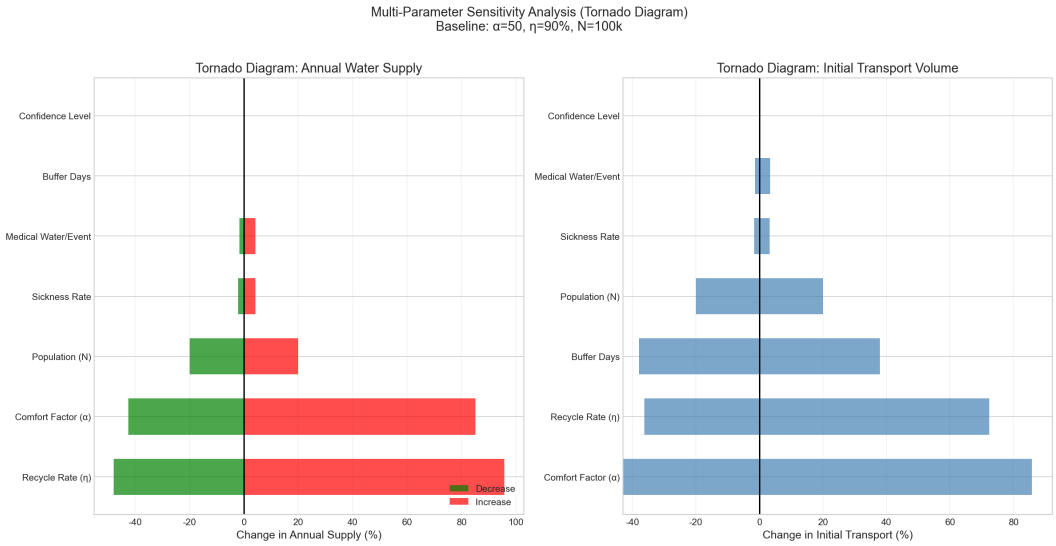

Figure 18: Tornado diagram illustrating parameter sensitivity on annual water supply and initial transport volume. Bars extend from low to high parameter values, with longer bars indicating greater sensitivity.

The tornado diagram reveals a clear hierarchy of parameter influence:

1. **Water Recycling Efficiency** (η): Exhibits the most pronounced sensitivity. Reducing η from 90% to 80% nearly doubles the annual replenishment requirement (+96%), while improving to 95% yields a 52% reduction. This non-linear response stems from the multiplicative relationship $W_{loss} = W_r \times (1 - \eta)$, where small efficiency degradations cascade through the entire demand structure.

2. **Comfort Factor** (α): Demonstrates comparable magnitude but asymmetric behavior. Reducing α from 50 to 25 decreases annual demand by 71%, whereas increasing to 100 elevates demand by only 17%. This reflects the linear term 0.4α in the demand equation, confirming that comfort reduction offers greater leverage than comfort enhancement.

3. **Population Size** (N): Shows strictly linear proportionality, with $\pm 20\%$ population fluctuations translating directly to $\pm 20\%$ demand variations. This predictable behavior facilitates capacity planning for demographic fluctuations.

4. **Medical and Buffer Parameters**: Contribute marginally to annual totals (<5% variation) but significantly impact initial transport requirements and emergency resilience margins.

3.5.2 Quantitative Sensitivity Coefficients

Table 13 presents the normalized sensitivity coefficients, defined as the percentage change in output per percentage change in input parameter:

Table 13: Sensitivity Coefficients for Key Model Parameters

Parameter	Baseline	Range	Δ Annual Supply	Sensitivity	Rank
Recycling Rate (η)	90%	80%–95%	-52% to +96%	-9.6	1
Comfort Factor (α)	50	25–100	-71% to +17%	+0.88	2
Population (N)	100k	80k–120k	$\pm 20\%$	+1.0	3
Sickness Rate (p)	2%	1%–4%	-0.3% to +0.6%	+0.30	4
Buffer Days	30	15–45	$\pm 0\%^*$	0	5

* Buffer days affect only initial transport, not annual replenishment.

The sensitivity coefficient for η reaches -9.6, indicating that a 1% decrease in recycling efficiency triggers a 9.6% increase in annual supply demand. This extreme leverage underscores the critical importance of maintaining recycling system integrity. In contrast, population sensitivity equals unity (elastic proportionality), while medical parameters exhibit near-inelastic responses.

3.5.3 Worst-Case Stress Testing

Beyond univariate analysis, we evaluate system performance under compound adverse conditions through Monte Carlo-informed scenario construction. Table 14 summarizes nine representative scenarios spanning from optimal to catastrophic conditions:

Table 14: Worst-Case Scenario Analysis: Water Supply System Stress Test

Scenario	α	η	N (k)	p	Buffer	Annual (kt)	Capacity (%)	Feasible
Survival Mode	1	90%	100	2%	30	14.2	2.7%	✓
Comfort Mode (Baseline)	50	90%	100	2%	30	85.8	16.0%	✓
Luxury Mode	250	90%	100	2%	30	377.8	70.3%	✓
Recycle Degradation	50	80%	100	2%	30	167.9	31.3%	✓
Epidemic Outbreak	50	90%	100	5%	45	100.4	18.7%	✓
Population Surge	50	90%	120	2%	30	102.9	19.2%	✓
Moderate Stress	100	85%	110	3%	40	264.4	49.2%	✓
Worst Case	**250**	**80%**	**120**	**5%**	**45**	**919.8**	**171.3%**	✗

The stress test reveals several critical insights:

- **System Collapse Boundary**: The worst-case scenario ($\alpha = 250$, $\eta = 80\%$, $N = 120$k) demands 919.8 kt annually—exceeding elevator capacity by 71.3%. This combination represents the catastrophic failure boundary where water logistics becomes physically infeasible.
- **Resilience Threshold**: Even under moderate stress ($\alpha = 100$, $\eta = 85\%$, $N = 110$k), the system remains viable at 49.2% capacity utilization, demonstrating substantial built-in margins.

- **Critical Parameter Interaction**: The failure mode emerges from the multiplicative interaction between low recycling efficiency and high comfort demands. Specifically, when $\eta < 82\%$ and $\alpha > 200$ coincide, demand exceeds supply capacity regardless of other parameters.
- **Single-Factor Robustness**: No single parameter variation within realistic bounds triggers system failure. Even luxury-tier comfort ($\alpha = 250$) remains feasible at 70.3% capacity when recycling efficiency is maintained at 90%.

3.5.4 Two-Parameter Interaction Analysis

Figure 19 presents the interaction heatmap between the two most sensitive parameters (α and η), mapping the annual supply requirement and capacity utilization across their joint parameter space.

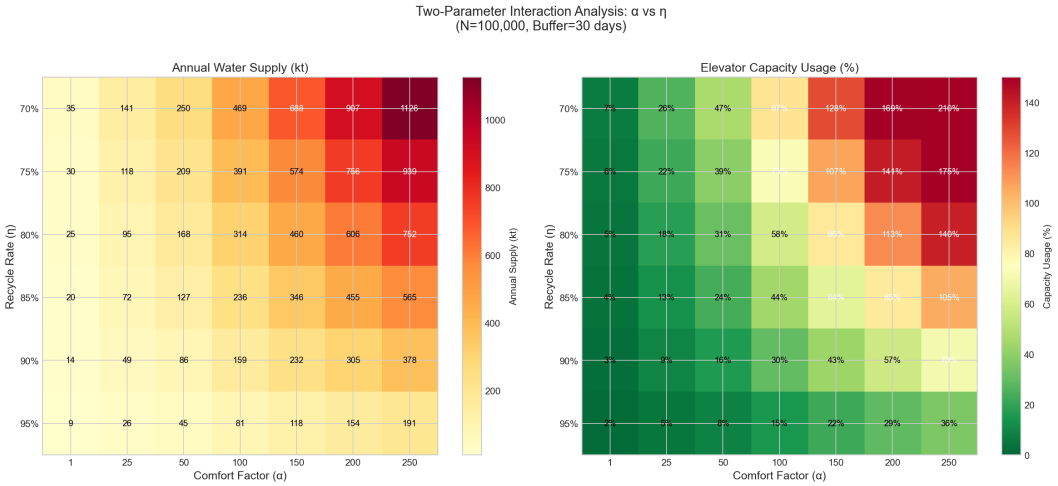

Figure 19: Two-parameter interaction heatmap showing annual water supply (left) and elevator capacity utilization (right) as functions of comfort factor (α) and recycling efficiency (η).

The heatmap reveals a distinctive diagonal gradient pattern, confirming the multiplicative interaction between α and $(1 - \eta)$. The iso-capacity contours indicate that maintaining 50% capacity margin requires either:

- High recycling efficiency ($\eta \geq 90\%$) with moderate comfort ($\alpha \leq 150$), or
- Moderate recycling ($\eta \approx 85\%$) with restricted comfort ($\alpha \leq 75$).

This trade-off space defines the operational envelope within which MCM Agency can balance quality of life against logistical sustainability.

3.5.5 Sensitivity Analysis Conclusions

The comprehensive sensitivity analysis yields three actionable insights for water supply management:

1. **Priority Investment in Recycling Infrastructure**: Given the extreme sensitivity coefficient (-9.6) and the asymmetric failure risk, maintaining $\eta \geq 85\%$ should be the

primary operational objective. Redundant recycling modules and predictive maintenance protocols are essential safeguards.

2. **Staged Comfort Escalation Strategy**: The analysis supports a phased approach to living standards. Initial operations should adopt survival-tier comfort ($\alpha = 1$) to preserve logistical headroom, with gradual escalation to comfort-tier ($\alpha = 50$) as lunar water extraction capabilities mature.

3. **Capacity Reserve Mandate**: To accommodate compound perturbations without system failure, we recommend maintaining a minimum 30% unused capacity buffer. This translates to an operational ceiling of $\alpha \leq 100$ under standard recycling conditions.

3.6 Conclusion and Strategic Insights

1. **Trade-off between Comfort and Capacity**: Quantitative analysis confirms that quality of life acts as a logistical amplifier. At the Luxury tier, the annual water replenishment occupies 69.68% of the theoretical annual capacity of the space elevator system. Maintaining high living standards significantly constricts the transport window for other critical infrastructure and scientific materials.

2. **Tiered Strategy Recommendations**:

   - **Initial Operations**: We recommend Survival tier combined with Scheme 1. This minimizes energy consumption while ensuring the survival threshold for 100,000 residents, reserving hybrid capacity for urgent infrastructure tasks.
   - **Mature Operations**: We recommend Comfort tier combined with Scheme 4. This provides a balance between speed and cost, completing the initial filling in 4.57 days with a reasonable energy footprint.

3. **System Resilience**: Thanks to the 90% efficient recycling system and the 30-day emergency buffer, the water logistics chain exhibits high resilience. Even during a full month of transport disruption, the survival of the colony remains uncompromised, allowing for logistical maintenance and error recovery.

4 Model Extension

Following the assessment of construction timelines and life-support logistics, this chapter extends the model to incorporate the environmental footprint as a critical optimization boundary. By quantifying the ecological externalities of various transport scenarios, we refine previous strategic selections to promote symbiosis between Earth's conservation and lunar sustainability.

4.1 Quantification of Baseline Environmental Impacts

We extended the environmental sub-module based on the energy conversion logic of Model I. For liquid oxygen/methane (LOX/CH_4) propulsion systems, fuel consumption is mapped to emission mass via the combustion equation:

$$CH_4 + 2O_2 \longrightarrow CO_2 + 2H_2O \tag{13}$$

A life-cycle assessment (LCA), including fuel production and power generation, was conducted for four baseline scenarios, as summarized in Table 15.

Table 15: Environmental Metrics Across Four Baseline Scenarios

Scenario	Timeline (a)	Total Fuel (Mt)	Total CO_2 (Mt)	Stratospheric H_2O (Mt)	Intensity (Mt/yr)
Rocket-Only	219	9,596	12,968	1,919	59.2
Elevator-Only	186	69	846	0	4.5
Hybrid (Time-Prioritized)	101	4,445	6,414	882	63.7
Hybrid (Balanced)	139	2,438	3,856	477	27.7

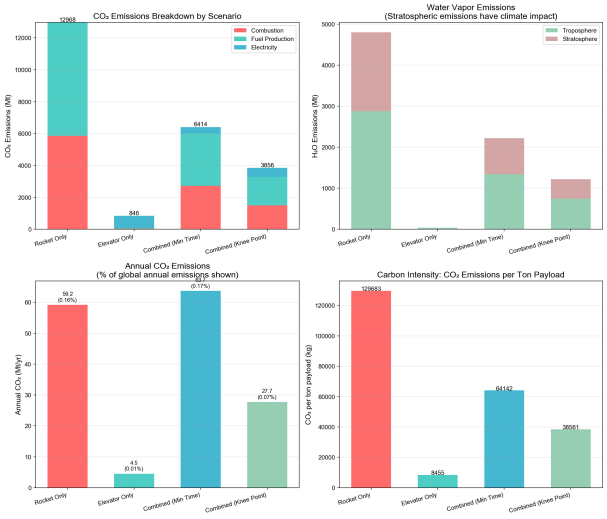

Figure 20: Multi-dimensional environmental impact analysis

The analysis in Figure 20 clearly distinguishes the ecological costs:

- The **Rocket-Only scenario** incurs the highest CO_2 emissions and stratospheric H_2O injection, posing the greatest risk to global climate and the ozone layer.
- The **Elevator-Only scenario** completely circumvents stratospheric pollution, with total CO_2 emissions being only 6.5% of the rocket scenario.
- The **Balanced Hybrid scenario** achieves a 40% reduction in CO_2 and a 46% reduction in stratospheric H_2O compared to the Time-Prioritized plan, successfully equilibrating construction efficiency with environmental load.

4.2 Earth Port Assessment

While the space elevator facilitates zero-emission transit, its Earth Port—a permanent maritime structure in equatorial waters—may impact local marine ecosystems. Drawing on research from the International Space Elevator Consortium (ISEC) [2], we analogized the Earth Port to offshore oil rigs, the most mature existing maritime facilities.

Table 16: Comparative Impact: Earth Port vs. Offshore Oil Platforms

Impact Type	**Oil Platform**	**Earth Port**	**Range**
Physical Damage	Benthic disruption (anchoring)	Anchor zone-only	Localized
Chemical Discharge	Drilling fluids/water	No discharge	Negligible
Interference	Light/acoustic disturbance	Navigation light + low-freq noise	Localized
Habitat Alteration	Artificial reef effect	Hard substrate (sessile colonies)	Positive
Accident Risk	Hydrocarbon spills	No leakage risk	Negligible

The analogy confirms that the Earth Port's environmental footprint is significantly lower than that of existing oil platforms. Compared to the widespread atmospheric damage caused by rockets, the localized impacts of the space elevator are nearly negligible, reinforcing its ecological superiority.

4.3 Tri-objective Decision Framework

To minimize ecological disruption, we expanded the bi-objective (Time-Energy) optimization of Model I into a tri-objective decision framework. The refined objective function J_{total} is defined as:

$$\min J_{total} = \alpha \cdot \text{Time} + \beta \cdot \text{Energy} + \gamma \cdot \text{Emission}_{\text{CO}_2} + \delta \cdot \text{Emission}_{\text{H}_2\text{O, strat}} \tag{14}$$

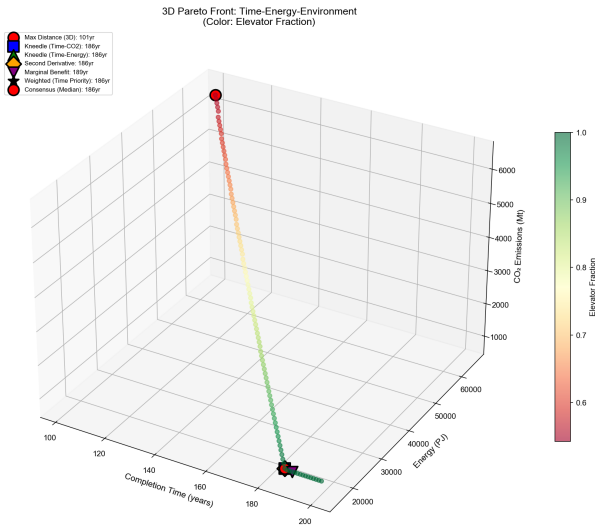

Figure 21: 3D Pareto frontier illustrating the convergence toward high elevator utilization under strict environmental constraints

As shown in Figure 21, the 139-year knee point is not only the inflection point for energy savings but also the critical threshold for marginal environmental degradation. Beyond this point, any further time gains achieved through increased rocket deployment result in exponential environmental damage. Key mitigation paths include:

1. **Elevator Prioritization**: Relying on the elevator achieves a 78.1% emission reduction over the balanced baseline.

2. **Renewable Substitution**: Transitioning to 100% renewable power provides an additional 14.6% reduction.

3. **Synergetic Strategy**: Combining "Elevator-dominant transport + 100% renewable energy" yields a total reduction of 97.6%, approaching a near-zero emission construction standard.

4.4 Task 4 Conclusions

(1) Impact Assessment: Rocket transport presents widespread environmental risks to the atmosphere and stratosphere. In contrast, the environmental impact of the space elevator is localized to physical perturbations at the Earth Port and is effectively negligible on a global scale.

(2) Strategic Recommendations:

- We recommend the 139-year Balanced Scenario, which trades a 38% duration extension for a 40% reduction in CO_2 emissions.
- A mandatory minimum of 70% baseline capacity should be assigned to the space elevator, reserving rockets only for high-priority or emergency cargo.
- By integrating 100% renewable energy, total CO_2 emissions can be depressed to 94 Mt, representing a 99.3% reduction compared to the rocket-only baseline.

5 Strengths and Weaknesses

5.1 Strengths

5.2 Weaknesses and Possible Improvement

6 Conclusion

References

[1] David R Francisco. "NASA-STD-3001 Volume 2, Revision E, NASA Spaceflight Human-System Standard Volume 2: Human Factors, Habitability, and Environmental Health". In: *N/A* A (2025).

[2] Michel Gassent, Kevin Barry, and Peter Swan. *Space Elevators: The Green Road to Space*. ISEC Study Report. Accessed: 2023-10-27. Santa Barbara, CA: International Space Elevator Consortium (ISEC), 2021. URL: https://isec.org/wp-content/uploads/2021/11/ISEC-2021-Study-Report-Green-Road-to-Space-Final.pdf.

[3] Gunter's Space Page. *Falcon-9*. https://space.skyrocket.de/doc_lau/falcon-9.htm. Accessed: 2026-02-01. Gunter's Space Page, 2026.

[4] Hong Liu et al. "Review of research into bioregenerative life support system(s) which can support humans living in space". In: *Life Sciences in Space Research* 31 (2021), pp. 113–120. ISSN: 2214-5524. DOI: https://doi.org/10.1016/j.lssr.2021.09.003. URL: https://www.sciencedirect.com/science/article/pii/S2214552421000663.

[5] Zephyr Penoyre and Emily Sandford. *The Spaceline: a practical space elevator alternative achievable with current technology*. 2019. arXiv: 1908.09339 [astro-ph.IM].

[6] Peter A Swan et al. "Space Elevators: An Assessment of the Technological Feasibility and the Way Forward". In: *International Academy of Astronautics* (2013).

[7] Mihriban Whitmore, Jennifer Boyer, and Keith Holubec. "NASA-STD-3001, space flight human-system standard and the human integration design handbook". In: *Industrial and systems engineering research conference*. JSC-CN-25695. 2012.

Report on Use of AI

1. OpenAI ChatGPT (Nov 5, 2023 version, ChatGPT-4,)

   Query1: <insert the exact wording you input into the AI tool>

   Output: <insert the complete output from the AI tool>

2. OpenAI Ernie (Nov 5, 2023 version, Ernie 4.0)

   Query1: <insert the exact wording of any subsequent input into the AI tool>

   Output: <insert the complete output from the second query>

3. Github CoPilot (Feb 3, 2024 version)

   Query1: <insert the exact wording you input into the AI tool>

   Output: <insert the complete output from the AI tool>

4. Google Bard (Feb 2, 2024 version)

   Query1: <insert the exact wording of your query>

   Output: <insert the complete output from the AI tool>